Soft Matter

Accepted Manuscript

This is an *Accepted Manuscript*, which has been through the Royal Society of Chemistry peer review process and has been accepted for publication.

Accepted Manuscripts are published online shortly after acceptance, before technical editing, formatting and proof reading. Using this free service, authors can make their results available to the community, in citable form, before we publish the edited article. We will replace this *Accepted Manuscript* with the edited and formatted *Advance Article* as soon as it is available.

You can find more information about *Accepted Manuscripts* in the Information for Authors.

Please note that technical editing may introduce minor changes to the text and/or graphics, which may alter content. The journal's standard Terms & Conditions and the Ethical guidelines still apply. In no event shall the Royal Society of Chemistry be held responsible for any errors or omissions in this *Accepted Manuscript* or any consequences arising from the use of any information it contains.

ROYAL SOCIETY OF CHEMISTRY

www.rsc.org/softmatter

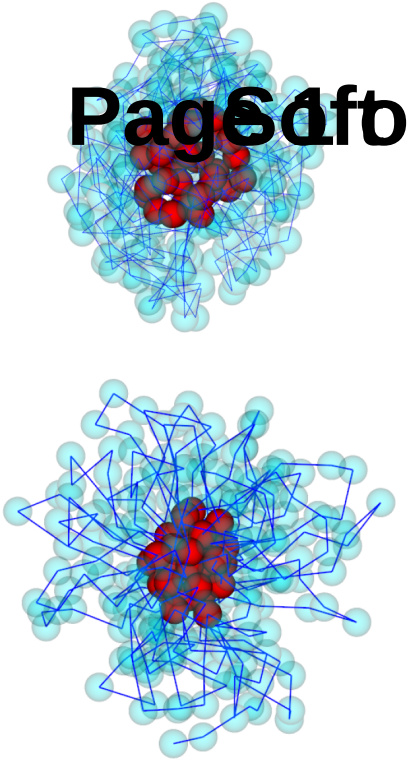

Soft Matter Accepted Manuscript

Switch-like polymer collapse and spontaneous domain formation in a polymer with sparse bridging and homogeneous self-adhesion.

Soft Matter Accepted Manuscript

ARTICLE TYPE www. rsc.org/xxxxxx | XXXXXXXX

Combined collapse by bridging and self-adhesion in a prototypical polymer model inspired by the bacterial nucleoid.

Vittore F. Scolari,[a,b,c,d] **Marco Cosentino Lagomarsino,**[*a,b]

Received Xth XXXXXXXXXX 20XX, Accepted Xth XXXXXXXXX 20XX
First published on the web Xth XXXXXXXXXX 200X
DOI: 10.1039/b000000x

Recent experimental results suggest that the *E. coli* chromosome feels a self-attracting interaction of osmotic origin, and is condensed in foci by bridging interactions. Motivated by these findings, we explore a generic modeling framework combining solely these two ingredients, in order to characterize their joint effects. Specifically, we study a simple polymer physics computational model with weak ubiquitous short-ranged self attraction and stronger sparse bridging interactions. Combining theoretical arguments and simulations, we study the general phenomenology of polymer collapse induced by these dual contributions, in the case of regularly-spaced bridging. Our results distinguish a regime of classical Flory-like coil-globule collapse dictated by the interplay of excluded volume and attractive energy and a switch-like collapse where bridging interactions compete with entropy loss terms from the looped arms of a star-like rosette. Additionally, we show that bridging can induce stable compartmentalized domains. In these configurations, different "cores" of bridging proteins are kept separated by star-like polymer loops in an entropically favorable multi-domain configuration, with a mechanism that parallels micellar polysoaps. Such compartmentalized domains are stable, and do not need any intra-specific interactions driving their segregation. Domains can be stable also in presence of uniform attraction, as long as the uniform collapse is above its theta point.

1 Introduction

It is now clear that bacterial chromosomes (which exist in the cell in a mesoscopic dynamic complex composed of DNA, RNA and proteins called nucleoid) are highly organized within cells. The conformational properties of the folded genome are essential for the processes of replication, transcription (and thus regulation of gene expression), and segregation [1–3].

Focusing on *E. coli*, the chromosome is a single circular molecule of about 4.7 million base pairs (Mbp) (≈ 1.5 mm) [4,5]. Nucleoid associated proteins, or "NAPs" (such as Dps and transcription factors Fis, H-NS, IHF, HU, and condensin MukBEF), can modify the shape of the DNA both at local and global levels [2,6,7]. Of particular interest are bridging interactions [8] (possible at least from Fis, H-NS, and MukBEF), which can in principle induce looped domain formation, through mechanisms that are believed to be important also for eukaryotic chromatin [9–11]. For example, a study combining super-resolution microscopy with genetic "chromosome-conformation capture" (3C) techniques on the NAP H-NS explicitly reported it to form a small set of foci in the cell, bringing together distant binding sites [12]. Additionally H-NS reduces the size of purified nucleoids [13]. RNA polymerase, the DNA-binding enzyme responsible for gene transcription, might also concentrate into transcription foci or "factories," affecting the nucleoid structure by bringing together distant loci [14,15].

The *E. coli* nucleoid, with a linear size of 1.5mm, occupies a well-defined region of the cell, with a volume of 0.1-0.2 μm^3 (the bare DNA volume is about a factor 20-30 smaller) [5]. Strong nucleoid compaction into a structure that does not fill the volume of the cell is experimentally observed *in vivo* [16,17]. The degree of compaction is modulated by the cell's growth conditions and in response to specific external cues. Rather than confinement from the cell boundaries, the dominant force for this compaction is likely to come from self-attraction due to molecular crowding and forces of entropic origin effectively causing a short-ranged self-attraction [18,19]. This self-adherent polymer organization is consistent with both *in vivo* observations [17,20] and *in vitro* experiments [21] with purified nucleoids. Note that compaction from bridging alone is not likely to be responsible of this behavior, as cytoplasm-free nucleoids are larger than cells, even if some NAPs are reported to stay bound [13,21,22]. Finally, a sub-Rouse viscoelastic dynamics of individual loci, whose mean apparent diffusion varies with chromosomal coordinates [23,24] suggests that (i) a simple polymer model is not likely to fully capture nucleoid organization

[a] *Sorbonne Universités, UPMC Univ Paris 06, UMR 7238, Computational and Quantitative Biology, 15 rue de l'École de Médecine Paris, France. Fax: +33 1 44 27 73 36; Tel: +33 1 44 27 73 41; E-mail: marco.cosentino-lagomarsino@upmc.fr*
[b] *CNRS, UMR 7238, Paris, France*
[c] *National Centre for Biological Sciences, Tata Institute of Fundamental Research, GKVK, Bellary Road, Bangalore 560065, India*
[d] *Manipal University, Manipal 576104, India*

Soft Matter Accepted Manuscript

(ii) the organization and dynamics of inter-loci tethering might also be complex.

Importantly, the state of the nucleoid is far from being an amorphous mass, randomly organized, such as e.g., one expects from a classical equilibrium collapsed globule[25]. On the contrary, the picture of a folded object with persistent (but dynamic) mesoscopic features, including a linear ordering of loci within the cell an overall coiled shape should be more realistic[17,20,21,26,27]. In these respects, one important reported feature of the *E. coli* chromosomes are the so-called "macrodomains"[28–30]. Often described as isolated compartments, such domains are roughly replichore-symmetric, i.e., mirror the order of replication of the *E. coli* genome, from the replication origin locus, oriC, to the terminus region, Ter). The first evidence for macrodomains[28] came from a non uniform pattern in the recombination frequency between chromosomal loci (which should be proportional to the population-averaged probability that the two chromosomal segments come into contact within the cell). Four macrodomains of a few hundred Kb in size have been identified, which divide the chromosome into six contiguous regions[1,31]. Subsequent studies have confirmed the presence of macrodomains using fluorescently labeled loci[30,32,33]. The Ter macrodomain appears to be condensed by a single DNA-binding NAP, MatP, which has a small set of specific binding sites in the Ter region[34]. A recent modeling study has implicated the differential condensation levels by macrodomains, together with the targeting of the Ori and Ter regions to specific subcellular positions, to the generation of the chromosome segregation pattern observed *in vivo*[35].

Additionally, nucleoids are composed of topologically unlinked dynamic domain structures, due to supercoiling (torsional constraints generated by active processes and frozen by bridging) forming plectonemes and toroids[4], and stabilized by nucleoid-associated proteins, such as Fis and H-NS. This combination of effects gives the chromosome a looped shape[36–38], where the loops form a tree of plectonemes. Supercoiling and nucleoid organization affect gene expression[2,36,39]. The level of supercoiling is tightly regulated by the cell, and it can be changed by the action of specific enzymes such as topoisomerases and gyrases.

Sequencing techniques (though relying on population averages) give further insight into the folding of bacterial chromosomes. High-throughput 3C techniques have been used to determine the global folding architecture of the *C. crescentus* swarmer cell genome[40,41], which is easier to access experimentally than *E. coli*, due to the well-characterized polar tethering of the chromosome and the more practicability of cell synchronization. These data show a chromosomal fiber-like organization, linearly ordered in a compressed ring-like fiber, and taking an eight shape inside the cell. Higher-resolution data[40] also show spatial domains of interacting, and exhibit a hierarchical nested organization over a range of length scales ($\sim 50-200$ Kb). These domains are stable throughout the cell cycle and are reestablished concomitantly with DNA replication. Additionally, domain boundaries co-occur with highly-expressed genes, and the domain organization is enabled by transcription. Such domains are hypothesized to be composed of transcription-induced supercoiled plectonemes arrayed into a "bottle brush" fiber. Regarding *E. coli*, the current resolution appears too low[42] to draw any specific conclusions, but finer-scale experiments are expected to appear soon.

While the bridging and loop-forming interactions are sometimes incorporated in polymer models of the bacterial chromosome[11,35,43–46], the standard approach is to neglect a possible self-adhesion and consider a confined polymer within the cell volume. Here, we set out to investigate how the combination of bridging and homogeneous collapse in a generic polymer physics (equilibrium) framework, using computer simulations and with the help of theoretical mean-field and scaling arguments. Rather than intending this as an explicit model for the chromosome, our intent is to generically explore the consequences of these two basic ingredients, in order to help more realistic model development and to link the phenomenology with the vast existing knowledge in polymer physics, and with chromosome models available in the literature[1,11,43]. In this spirit, we deliberately ignore the role of supercoiling, and we do not consider confinement. We also neglect segregation dynamics and other non-equilibrium drives (see the Discussion). Our main results are a qualitative characterization of the state diagram of this model, where we observe a sharp collapse to a rosette-like state where bridging interactions overcome entropy loss by loops. This collapse can be described by classical Flory-like mean-field arguments only when the density of bridges is sufficiently high, and homogeneous self-attraction modulates the collapse by affecting the interactions between rosette arms. Finally we find that bridging can form multiple rosette domains, which are stable under a wide set of conditions and whose number is set by the model parameters.

2 Model

The basic ingredients of the model are illustrated in Fig. 1. Our simulation uses a simple off-lattice Monte Carlo algorithm with Metropolis rejection rule. The algorithm is a variant of the "bead-spring" polymer model used in ref.[47]. The polymer is represented as a linear string of N spherical "beads" of diameter σ, connected by bonds of maximal extension $\lambda \geq \sigma$. We simulated polymers composed of up to 512 beads. All monomers interact via a hard-core repulsion potential

$$U_r(r_{ij}) = \begin{cases} 0, & \text{if } r_{ij} > \sigma \\ \infty, & \text{if } r_{ij} \leq \sigma \, . \end{cases}$$

Soft Matter Accepted Manuscript

This journal is © The Royal Society of Chemistry [year]

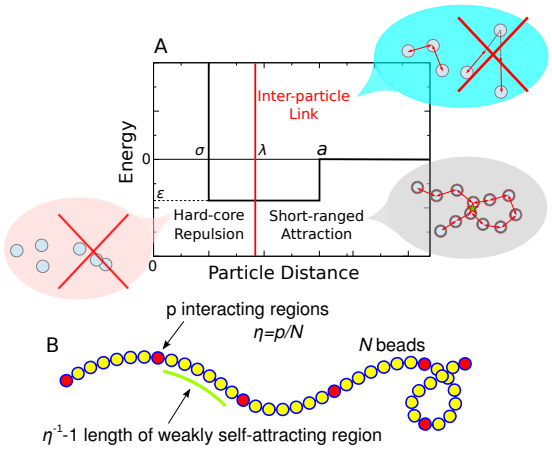

Fig. 1 Illustration of the model. A: The interparticle potential comprises a hard-core repulsion between all discretization "beads" of the polymer (whose range is set by the parameter σ), and a short-ranged attraction potential of range a and depth ε_u for the homogeneous self-attraction (acting on all beads) and ε_l for the sparse bridging interactions. Additionally, consecutive beads are subject to a maximum separation hard constraint of length λ. B: Parametrization of the position of bridging interactions. A total of p bridging beads are placed across p equally spaced regions of length $\simeq N/p$. The beads in the interspersing regions only feel the weaker self-attraction of energy ε_u.

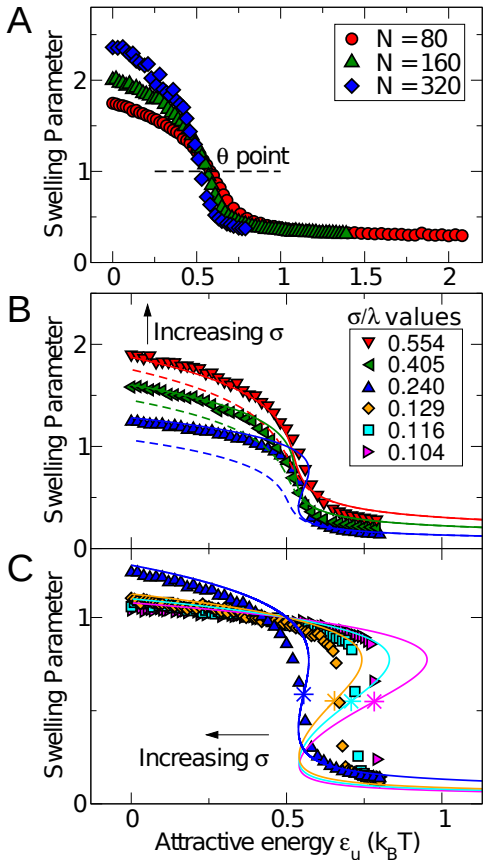

Fig. 2 Collapse under homogeneous short-ranged attraction and Flory mean-field theory. A: Collapse curve of the swelling parameter α, plotted as a function of the attraction energy ε_u, for different values of N. In order to keep the swelling parameter constant in the collapsed phase, we set $\sigma = 0.29N^{1/6}\lambda$ inthese simulations. B and C: Comparison of collapse curves with mean-field theory for polymers with different excluded volume (varying σ/λ) at fixed $N = 320$. Solid lines are solutions of the modified mean-field theory, Eq. (1), while dashed lines are solutions of the Flory mean-field theory. Panel C shows that for smaller values of σ/λ the inflexion point of the collapse curve becomes very steep, and moves towards larger values of ε_u energy. This feature is qualitatively captured by the modified Flory mean-field theory. The numerical collapse points matched the reentrant inflexion points of the theoretical curves, indicated by stars on the solid lines in the plot.

Additionally, consecutive monomers feel the nearest-neighbor bonds as

$$U_b(r_{i,i+1}) = \begin{cases} \infty, & \text{if } r_{i,i+1} > \lambda \\ 0, & \text{if } r_{i,i+1} \leq \lambda \end{cases} .$$

The short-ranged attraction, applied between all monomers, is modeled as a negative square well between the two bounds imposed by the two above potentials, and within a maximum range of $a = 1.44\sigma$ (Fig 1A). The depth of the attractive potential is ε_u for all beads, modeling a generic short-ranged attraction due to depletion effects / molecular crowding[48]. Bridging interactions are modeled as sparsely chosen beads with additional square-well attractive potentials of the same range, but acting only on other beads of the same class with interaction energy ε_l. Fig. 1B illustrates the criteria for placing the bridging interactions and their parametrization. We considered a situation where bridging beads are equally spaced, in number p; $\eta = p/N$ is the total fraction of beads occupied by the bridging regions. We are especially interested in the regime where p is fairly small (note that in this regime the value of p may be explicitly relevant, and consequently we will not refer to η alone as the control parameter).

3 Results

Collapse from homogeneous self-attraction.

As a test scenario of the simulation, we first considered the limit case of collapse of a simple polymer with homogeneous self-attraction (a homopolymer). In this case one expects to find the conventional theta transition, and this is the case in our simulations. To show this, we considered the swelling pa-

Soft Matter Accepted Manuscript

rameter α, defined here as the ratio of the mean end-to-end distance of the polymer $R_e = \langle|\mathbf{r}_N - \mathbf{r}_1|\rangle$ in a given condition and its value $R_0 = \lambda \left(\frac{3}{5}N\right)^{1/2}$ at the theta point. Fig. 2A shows a plot of this quantity as a function of the homogeneous attraction energy per bead ε_u, for polymers with increasing N. The theta point is located where the swelling parameter equals one. We verified that its position corresponds well to the prediction of the Flory mean-field theory, which defines the theta point from the balancing, in the second virial coefficient, of the excluded volume interaction term with the attraction term. In our case both terms can be estimated from the Mayer function, respectively as $v_1 = \frac{4}{3}\pi\sigma^3$ (repulsion) and $v_2 = \frac{4}{3}\pi\beta\varepsilon_u(a^3 - \sigma^3)$ (attraction), with $\beta = 1/(k_B T)$.

In our simulations, the shape of the collapse curves of the swelling parameter changes with varying excluded volume, i.e. varying σ (at constant $\lambda > \sigma$). As σ increases, the theta point correctly shifts towards larger energy values (Fig. 2B and 2C). However, for increasingly "thin" polymers, while the theta point still follows the predicted behavior, the inflexion point of the swelling ratio plotted as a function of ε_u becomes very steep, and radically moves towards increasingly larger values of ε_u instead of smaller ones. These values, and not the theta point, correspond to where the "collapse", intended as a major jump in the swelling ratio, effectively takes place. This phenomenology has been reported previously[49], and may correspond to a first-order transition related to polymer crystallization[50]. We report this in order to avoid confusion between this sharp collapse and one of our main results, where a sharp transition is due to bridging only. In the following we will restrict ourselves to parameter values $\sigma = 0.424\,\lambda$ for $N = 256$, where this kind of sharp collapse phenomenology due to small σ/λ *does not* occur.

The commonly used way to find the globule size and reproduce the collapse curve by a Flory-like mean-field theory is to counterbalance the two-body interaction term described above with a three-body excluded volume term. We find improved agreement with the following variant[49]

$$\beta F = 3[\alpha^2/2 - log\alpha] + 3N/5[v\rho + B_3\rho^2]\,, \qquad (1)$$

where $\rho = N/R^3$ is the concentration, $v = v_1 - v_2$ plays the role of an effective "excluded volume" parameter and $B_3 = (v_1)^2/6$. Note the logarithmic entropic term, which can be understood as coming from the prefactor of the radial distribution of a freely-jointed chain. This term becomes relevant for $\alpha < 1$ and its addition captures rather efficiently the simulation behavior described above (Fig. 2B). For extremely small excluded volumes, the reentrant inflexion points of the theoretical collapse curve appear to match rather well (Fig. 2C) the collapse points observed in our simulations.

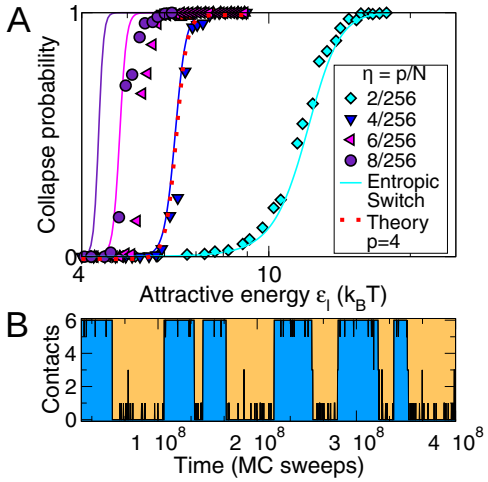

Fig. 3 Collapse due to bridging proteins. A: Switch-like transition to a collapsed rosette-like state for polymers for small numbers of bridging interactions p, solid lines (—) show the predictions of the theoretical estimates assuming two states (Eq.4), while red dots (···) correspond to the full estimate for $p = 4$ (Eq. 3), both taking into account the measured scaling $P_{(\mathrm{loop})} \sim g^{-2.27}$. The star polymer contribution has been neglected (see Fig. 8). B: Two-state dynamics of the number of active bridging interactions (contacts) for $p = 4$. The interaction energy $\varepsilon_l = 6.52 k_B T$ is set close to the critical value measured in panel A. The plot shows switching between a compact and a swollen state as a function of Monte Carlo time, compatibly with a first-order phase transition showing phase coexistence between a completely collapsed state (with six contacts) and the swollen state.

Collapse in presence of bridging interactions

We now discuss the case of collapse driven by sparse bridging interactions only ($\varepsilon_u = 0$). This case is sometimes presented as analogous to the classical collapse transition of a homopolymer[11,43]. While we confirm this analogy, we also find that there are important physical differences between the two situations. The conventional theta point and collapse are determined essentially by a balance between excluded volume and attractive interaction. In presence of sparse bridging points, the relevant contribution to the partition function balanced by attractive energy is not monomer excluded volume, but rather the entropy reduction for closing loops between bridging points[51] (this kind of switch-like looping transition has also been studied in the context of transcriptional regulation[52]). In order to show this, we have considered explicitly the following simplified partition function[51,52],

$$Z = \sum_C d_C e^{\beta n_b^{(C)} \varepsilon_l - \Delta S(C)}\,, \qquad (2)$$

where C runs over the possible bridging states, with degeneracy d_C and n_b is the number of bridging interactions in a given

Soft Matter Accepted Manuscript

This journal is © The Royal Society of Chemistry [year]

configuration. For small p this can be estimated as the number of pairs of interacting bridging monomers. For example, for $p=4$, $n_b^{(\min)}=0$, and $n_b^{(\max)}=6$ (i.e. $n_b^{(\max)}=p(p-1)/2$). For large cores of bridging beads, the effects of hard core repulsion and finite-length attractive interactions make this term linear in p (proportional to the core volume). We suppose that there is only one "fully collapsed" state C^* where the bridging interactions are concentrated in a spherical shaped core (we neglect for the moment surface effects in the core, see below). The probability for such state is

$$P(C^*) = Z^{-1} e^{\beta n_b^{(\max)} \varepsilon_l - \Delta S(C^*)} . \quad (3)$$

To estimate the entropy loss contributions for each loop, we use the first return probability for the polymer of length $g=(N-p)/p$. This can be estimated for large g as the return probability of a random walk. i.e. $P_{(\text{loop})} \simeq (a^3/\lambda^3) g^{-3/2}$; this approximation is correct for ghost polymers while the scaling for the swollen state is $P_{(\text{loop})} \sim g^{-2.27}$[51]. While the entropy of many configurations can be estimated as a combination of loops of varying length, complex constrained configurations can emerge that are not reducible to simple loops, but the entropy loss terms can be computed case by case in a straightforward way (for example for $p=4$ only one such configuration emerges, connecting bridging points 1-3 and 2-4). Fig. 3A shows a comparison of the calculation carried out for $p=4$, and direct simulation. The agreement between the estimated and measured $P(C^*)$ is satisfactory, indicating that indeed a loop entropy reduction switch is relevant.

Additionally, we find that for p sufficiently small, the dominant contribution to the estimate is the collapsed state C^*, and the transition can be captured by a simplified two-state partition function keeping into account only the fully unfolded and the fully bridged configurations (Fig. 3A),

$$Z_R = (p-1)! + P_{\text{loop}}(g)^{p-1} e^{\beta \varepsilon_l n_b^{(\max)}} , \quad (4)$$

obtained from equation 2 and 3 with $\Delta S(C^*) = (p-1)\log\left[P_{\text{loop}}(g)\right]$. The prediction looses quantitative precision for increasing p, due to the fact that the entropy reduction due to interactions between loops[53] is neglected. We verified that the estimate is accurate for a ghost chain, and produced a refined estimate keeping into account the star-polymer contributions at scaling level (see Appendix A and Fig. 8AB). Altogether, this evidence supports the picture of a switch-like transition to a rosette state, driven by the competition between bridging attraction and looping entropy, and somewhat reminiscent of microphase separation in diblock copolymers[54].

Fig 4A shows the observed collapse curves for the swelling ratio for different numbers of bridging interactions p at fixed N. We noted that, for small p, the transition points show better agreement if one uses the total energy ($p\varepsilon_l$) as control parameter, rather than using $1/\eta = p/N$ as rescaling factor for ε_l,

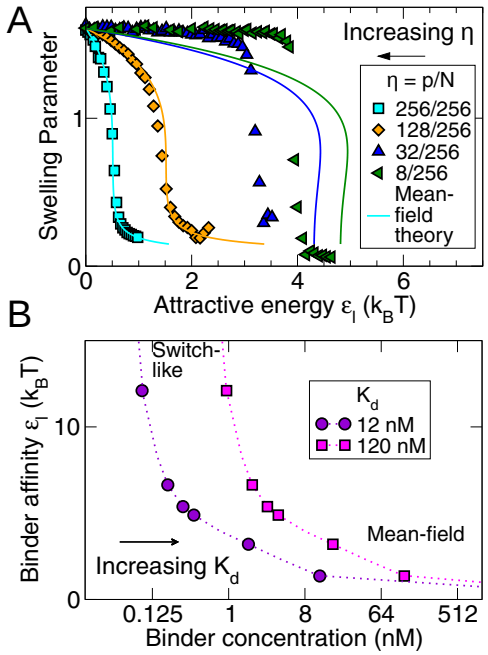

Fig. 4 Collapse due to bridging proteins. A: Collapse curves (swelling parameter vs ε_l) plotted for large p (and η); the transition energy moves to lower values for decreasing p (coded by color and symbols, see legend), the case $p/N=1$ corresponds to the case of uniform collapse. The parameters have been chosen so that the phenomenology of Fig. 2C is not present. The solid lines are fits from the Flory-like theory (Eq. 1) on the parameters β and B_3, showing that the theory works for large $\eta = p/N$ only. B: Transition energy plotted as a function of an effective concentration of bridging proteins, estimated from p,N, by a Langmuir model at equilibrium. We assumed different effective dissociation constants K_d for the binders with a range of values typical for transcription factors[57] (1 to 500 nM). Dashed lines are guides to the eye. The region of low binder concentration is expected to produce a switch-like transition to a rosette state, while the high-concentration regime is expected to follow Flory-like mean-field behavior. An increase of K_d corresponds to a rescaling of the transition curve. Simulations were performed using 256 beads and varying $p, \varepsilon_u, \varepsilon_l$, with typical thermalization times of $1.2 \cdot 10^7$ Monte Carlo sweeps.

confirming that for small p, η and p are not equivalent (in the thermodynamic limit, p has to be linear in N in order to observe collapse[55,56]). Close to the critical point, the dynamics of the swelling parameter as a function of Monte Carlo time shows switching between two well-defined states (Fig. 3B), a swollen one and a compact rosette-like one. This suggests that the switch-like transition is likely first order (similarly to the transitions observed in diblock copolymers).

Importantly, there is a crossover between this likely first-order and the Flory-like (second order) homopolymer collapse behavior (as shown in Fig. 2), when η and p are sufficiently large. Camacho and Schanke[56], working on a very simi-

Soft Matter Accepted Manuscript

lar system, suggested the possibility of a first-order collapse transition for sparse bridging, changing to second order for $\eta \simeq 0.6$. We were not able in this study to explore systematically this crossover, which resembles a standard second-order collapse for values of $\eta = p/N$ greater than $0.3-0.4$. However, we are not aware of existing studies fully characterizing the crossover between the switch-like transition driven by loop entropy and the Flory-like collapse. A less exotic possibility is that (as in a liquid-gas phase transition) in the thermodynamic limit the transition is always first-order, unless $\eta = 1$.

Finally, Fig. 4B makes a parallel between the case of sparse bridging interactions with no homogeneous self-attraction, and the "strings and binders switch" (SBS) model used in the context of eukaryotic chromatin [10,46]. The only difference between the two situations is that in the SBS model a pre-defined set of sparse bridging interactions can be occupied or not by a gas of bridging binders, while the set of bridging locations is fixed in the model considered here. To produce an estimate mapping the two situations, we considered a Langmuir process, and assumed it to be in chemical equilibrium. This procedure gives a mean value of p corresponding to a binder concentration, depending on the dissociation constant K_d of the binders (we assumed K_d within the range of values typical of transcription factors [57], around 1 to 500 nM). Specifically, $p \simeq N/(1+K_d/c)$, where c is the concentration of binders. We find that this rough estimate leads to a state diagram that reproduces qualitatively the features of the SBS model (Fig. 4B).

Combination of sparse and homogeneous interactions We now consider the case of collapse driven by both sparse bridging interactions and homogeneous self-attraction ($\varepsilon_u > 0$). The configurations of the polymer under these conditions are subject to at least two different regimes, corresponding to the conditions in which homogeneous interactions are large or small with respect to the collapse energy for the homopolymer alone (we assume in both cases that the bridging interactions are stronger $\varepsilon_l > \varepsilon_u$). Fig. 5B shows different collapse curves for the swelling ratio of the polymer in the two regimes, for $p/N = 8/256$. In the regime where the loops of the rosette are swollen ($v > 0$) the collapse is driven by the homogeneous interactions while in the regime where the arms are collapsed ($v < 0$) this does not happen.

For the swollen arms case, increasing uniform self-attraction (i.e. increasing ε_u) also shifts the observed transition point ${\varepsilon_l}^*|_{\varepsilon_> \varepsilon_u^*}$ towards lower values (see Fig. 5B). The largest contribution to this shift comes from the reduced excluded volume interactions between the looping chains (lower v). This shift reflects partially the effect of adding the contribution of the uniform interactions directly on the bridging beads, but we verified that this contribution is considerably smaller. As previously observed [58], the collapse curve for increasing ε_u in the first regime resembles the collapse of a homopolymer even

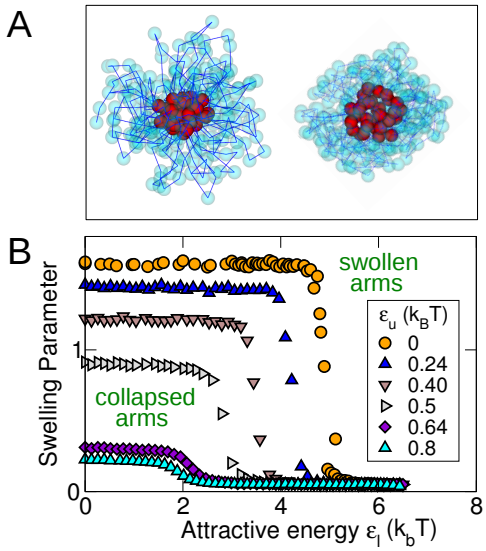

Fig. 5 Combined effects of bridging interactions and homogeneous self-attraction. A: Snapshots of typical simulated collapsed configurations with bridging interaction stronger than uniform self-attraction. Left: the collapse is driven by bridging, while the rest of the polymer forms closed swollen loops. Right: if ε_u is sufficiently large, both core of bridging beads and looped arms are collapsed. B: collapse curves (swelling ratio α vs ε_l) shown for different values of ε_u (coded by color and symbols, see legend) and $p/N = 8/256$. For larger values of homogeneous attraction energy ε_u which put the homogeneous part of the polymer below the theta point, the formation of a core of the bridging proteins still occurs inside the formed globule, but the point at which this occurs ${\varepsilon_l}^*|_{\varepsilon_u > \varepsilon_u^*} \simeq 2k_BT$ appears to depend only weakly on ε_u. Simulations were performed with $N = 256$ and $p = 8$ for $7.5 \cdot 10^8$ Monte Carlo sweeps, and with varying values of ε_u and ε_l (see legend).

in the presence of a small fraction of monomers which interact more strongly. Fig. 5B shows that the effect of bridging interactions on the swelling ratio is negligible before a critical energy ${\varepsilon_l}^*|_{\varepsilon_u > \varepsilon_u^*} \simeq 2k_BT$, which depends on p, where the bridging interactions form a core at the center of the globule. This effect modifies the swelling ratio (defined from the end-to-end vector) since the end beads are bridging.

The dependency of the free energy in the looped chains from the excluded volume coefficient v can be estimated by the analogy of the rosette-like collapsed conformation to a star polymer with $f \simeq p$ arms. Following Daoud and Cotton [59] (see Appendix B), we estimate this entropic contribution to the free energy to scale as

$$\beta F_{(\text{corona})} \sim f^{3/2} \log \left(N f^{7/6} v^{1/3} \left(\frac{b}{r_0} \right)^{5/3} \right) , \qquad (5)$$

for $v > 0$ where b is the monomer size and r_0 the size of the core. Inserting Eq. (5) as additional term in the mean-field

Soft Matter Accepted Manuscript

This journal is © The Royal Society of Chemistry [year]

theory leads to predict a logarithmic shift of the transition point from $v = 0$, which is consistent with simulated data (see Fig. 5B and Fig. 8C).

Compartmentalization

Intriguingly, we find that the switch-like collapse, in the presence of sparse interactions can lead to long-lived states where *multiple* collapsed micelle-like domains coexist. Fig. 6A shows snapshots of such configurations. Multiple domains are also visible from interaction maps, i.e. tables where the indexes are the discrete arc-length coordinates of the polymer beads and the entries are proportional to the mean-square distances between beads with given coordinates (Fig. 6AB). States with multiple domains were stable in our simulations for as long as we could measure. Additionally, states prepared with the initial conditions of a single domain would switch to a two- or three-domain state, which was then observed to be stable (Fig. 6B). This observation leads us to believe that the multi-domain configurations might not be metastable, but true equilibrium states. Additionally, the states can be still observed in presence of homogeneous self-attraction, i.e. for $\varepsilon_u > 0$, and the existence of such states affects the size and the shape anisotropy of the collapsed globules, measured as the ratio between the first and the third eigenvalue of the polymer's inertia matrix (Fig. 7). This analysis suggests that the elongated multi-domain configurations can be stable only if ε_u is such that the polymer arms are above their theta point.

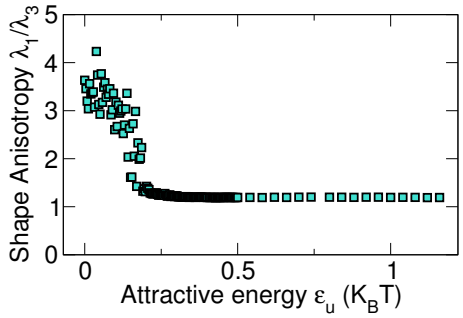

Fig. 7 The shape anisotropy due to multiple domains (measured as the ratio between the first and the third eigenvalue of the inertia matrix) shows a transition when the attractive energy ε_u crosses a threshold. The transition is due to coalescence of multiple domains. Simulations are performed with $N = 512$, $\sigma = 0.474\,\lambda$, $p = 32$.

In order to argue that multi-domain states could be stable, we rely on the following scaling argument, related to the case of polysoaps[60,61]. We consider a configuration with q domains, made of a "core" of p/q bridging monomers and a "corona" of $p - 1 \simeq p/q$ loops. Treating the loops of each domain as a star polymer[60] with $f = p/q$ "arms", and considering the leading contribution to the entropy scaling $f^{3/2}$[59] leads to estimate the free energy change by subdivision into q domains as

$$\Delta F_{(\text{corona})} \sim p^{3/2} q^{-1/2} \tag{6}$$

The remaining relevant terms in the free energy are energetic, and contain a core volume term (proportional to ε_l) which is not affected by the partitioning the polymer into domains, and the surface tension term leading to the change

$$\Delta F_{(\text{core})} \sim \varepsilon_l (p)^{2/3} q^{1/3} \,. \tag{7}$$

Minimizing the two contributions with respect to q (assumed continuous) leads to the expected equilibrium number of domains

$$q_{\text{eq}} \sim p \varepsilon_l^{-6/5} \,, \tag{8}$$

indicating that the number of stable domains should increase for larger p and decrease if ε_l is too large.

This behavior is observed in our simulations. However, this argument can be regarded as only qualitative. For example, the estimate in Eq. (5), since $r_0 \sim q^{1/3}$ implies $\Delta F_{(\text{corona})} \sim p^{3/2} q^{-1/2} \log\left(p^{5/3} q^{-2/3}\right)$, which (even neglecting prefactors) affects the predicted scaling. Additionally, the argument for the entropy is consistent only when the arms are above the theta point ($v > 0$). Note that, differently from the case of polysoaps, the multi-domain states in this picture are due to the trade-off between the energetic cost of the core surface when making multiple domains and the entropy increase due to making star-like configurations with an increasing number of arms. Hence, according to the argument, a multi-domain state is stable because partitioning $(p-1)$ arms into more than one domain is less costly compared to the energy cost of partitioning the bridging proteins in multiple domains. Finally, for large cores, an additional contribution to the entropy can be expected from the non-bridging beads that are "buried" in the core because of their vicinity to bridging beads. The most naive estimate for this additional cost for core size assumes that if a bridging bead is at position $r < r_0$ within the core, it brings in $(r_0 - r)^2$ beads (i.e. buried beads will behave like a theta-point polymer within the core). since there are order r^2 beads in each shell of the core, integrating along the radial coordinate will make the cost scale as r_0^5 (i.e. $p^{5/3}$) explicitly favoring fragmentation into multiple domains. While this effect might only need to quantitative corrections in our simulations (since typically p is small), it might be important in realistic situations.

4 Discussion and Conclusions.

We have analyzed a generic model of polymer collapse driven by a combination of homogeneous and sparse attractive interactions. Quantitative scaling arguments and simulation in

Soft Matter Accepted Manuscript

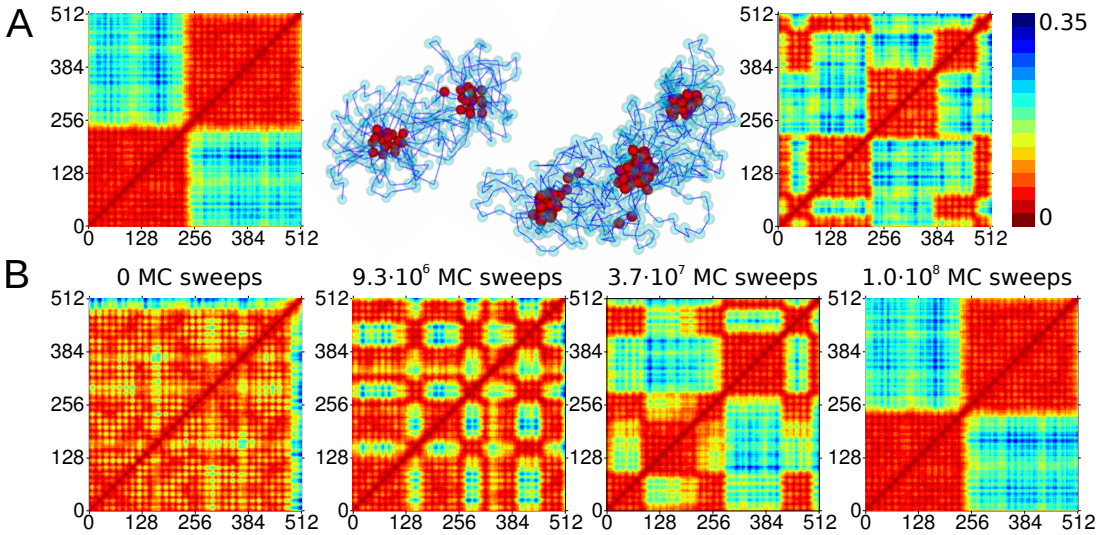

Fig. 6 Self-assembled micro-segregation into domains and shape anisotropy. A: Snapshots and colormaps of mean-square distance between polymer segments (in units of R_0^2) shown for typical two-domain (left, $\varepsilon_l + \varepsilon_u = 2.4$, $\varepsilon_u = 0.15$, 10^8 Monte Carlo sweeps) and three-domain (right, $\varepsilon_l + \varepsilon_u = 2.4$, $\varepsilon_u = 0.005$, 10^7 Monte Carlo sweeps) stable configurations; multiple domains are stable due the entropic repulsion of the loops arranged in a star-like configuration. B: Stability of multi-domain configurations over single-domain collapsed state. The interaction maps of panel A are shown for increasing Monte Carlo times. The initial configuration of the simulation prepared as a single domain (left, as in Fig. 5A), after $9.3 \cdot 10^6$ and $3.7 \cdot 10^7$ Monte Carlo sweeps the system (parameters as in panel A) shows a disintegration of the single-domain configuration and a progressive reordering of the stable configuration in distinct clusters (middle), (right) at 10^8 sweeps a two-domain configuration is stable. Simulations are performed with $N = 512$, $\sigma = 0.474\,\lambda$, $p = 32$.

parallel allowed us to access some basic aspects of the equilibrium behavior of this system. There are two main results. First, we find a crossover between Flory-like collapse and a switch-like, presumably first-order compaction where bridging counterbalances loop formation. Both phenomenologies often feature as ingredients of simple physical models for chromatin[9,10,25,51,62], but the interplay between the two is relatively inexplored. Second, states with multiple micelle-like domains can exist, in a manner that is reminiscent of micellar polysoaps[61]. We find that such multi-domain states are stable: similar conclusions were reached by a recent study of a polymer model with sparse bridging interactions, motivated by transcription factories[11], and motivated with a Flory-like theory for a macroscopic extended network of foci. To explain these structures, our work takes the complementary approach of considering the stability of star-like rosettes. Similar patterning (with a more complex phase diagram) has been observed in colloidal systems driven by an external force towards a surface with grafted polymers[63] or in sandwiched polymer brushes[64]. While the phenomenology is interesting, the latter case seems particularly interesting from the physics viewpoint because all the main driving forces have entropic origin.

Both of our main results are backed a series of simple mean-field/scaling arguments. While little of this knowledge can be called radically new, our combined simulation and analytical approach helps linking the results with generic knowledge in different sectors of the polymer physics literature, including mean-field and micelle-like collapse[49,51], polysoaps[61], star polymers[53,59]). Overall, we believe that there is an importance in elucidating these links, especially because they are not always kept into account in the current landscape of models of (bacterial) chromatin[1,43]. Interestingly, the difference between "homogeneous" (Flory-like) and "heterogeneous" (switch-like) collapse has been explored in the 1990s with the motivation of protein folding[55,56,65]. Dynamically, they are related to the difference between "downhill" folding, where large gains in stabilizing energy and loss in conformational entropy are balanced in a way that a large range of structures can be observed at the same time, and "two-state" folding, where intermediate structures do not matter. Biologically, one can imagine that the collapse and swelling of genomic regions may be tuned to be switch-like or second order, in order to be differentially controlled externally by the cell. Additionally, theoretical arguments are useful to elucidate the main ingredients causing a specific effect. In particular, they lead us to speculate that the stability of multi-micelle configurations is conferred by the competition between surface tension of the core and the entropic cost of the corona, which is similar to a

Soft Matter Accepted Manuscript

This journal is © The Royal Society of Chemistry [year]

star polymer. Our simulation results appear to be in line with this hypothesis. A further entropic cost due to burial of non-bridging bonds in the core is speculated to play a role for large cores. In analogy with diblock copolymers, one can speculate the existence of more complex micellar phases, for example with cylindrical symmetry, which might be exploited biologically. Overall, compared to previous literature, our work provides a more precise analysis of the collapse transitions by comparing simulations in different regimes and discusses in some more detail the orders of transitions. Additionally, we address the role of homogeneous self-attraction, which is usually disregarded in studies motivated by genome organization.

The model explored here is solely based on self-adhesion and bridging, as motivated by recent observations on bacterial chromatin. Other possibly important factors were voluntarily left out, in order to obtain a cleaner description of theoretical consequences of these two ingredients. A possibly very important feature of bacterial chromosomes disregarded by this model is the role of supercoiling, and the effectively branched structure of plectonemes. Modeling work on *Caulobacter*[40] supports the hypothesis that supercoil loops induced by transcription, using an effective numerical description of supercoil-induced branching. A more detailed model indicates that supercoiling facilitates the probability of protein-induced bridging[66]. Regarding the specific findings reported here, on the light of these studies we believe that a branched structure induced by supercoiling could modulate both the loop formation entropy and the loop-loop interaction entropy, thus affecting both the contact map and the polymer size at fixed conditions. Due to limitations of our simulation technique, we also left out from this modeling framework topological constraints, which have been implicated for eukaryotes[25,67]. Such constraints lead to long-lived metastable states in a collapsing polymer or a melt of rings, characterized by a dense fractal-like organization (and in contrast with the dense but non-fractal organization of an equilibrium globule). We have previously hypothesized[1] that the peculiar sub-diffusive dynamics of *E. coli* chromosomal loci[23,24] might be connected to this kind of organization.

It would be premature to draw any clearcut biological conclusions based on this simple model regarding phenomena occurring in real chromosomes. The main biological insights of this work are the generic notions that the features and even nature of the collapse transition may be tunable by modulating the sparsity of bridging and the homogeneous self-adhesion, and that the tendency to form domains could be intrinsic of the bridging (and tuned by the osmotic self-adhesion), and require in principle little or no inter-specificity of domains[46]. This block-copolymer-like behavior could be generally interesting in the context of eukaryotic chromatin. For example, mutually repellent rosette-like chromosomal structures are also observed in some plants and also lead to chromosome territories[68], and bottle-brush structures are common in meiotic chromosomes[69]. In bacteria, this kind of spontaneous sorting mechanism might play a role in the observed correlation between the position of genetic loci along the chromosome and their position in the cell[27,34], and possibly also in the resolution of the identity of segregating sister chromosomes[35,70]. More speculatively, the tunable transition observed here suggests a possible more general link between the behavior of the bacterial nucleoid and the technological area of "smart", or stimulus-responsive polymers[64,71]. These are polymer systems (e.g. films or polymer-colloid mixtures) designed to show a variety of responsive behaviors to external stimuli such as light, chemicals, and solvency. Similar "intelligent" behavior could be shaped into nucleoids by natural selection, and serve biological purposes such as physiological response on fast time-scales.

5 Acknowledgments

We are very grateful to Peter Olmsted for pointing to our attention the literature on polysoaps, to Anton Goloborodko for suggesting the contribution of buried beads to the core entropy, Leonid Mirny, Marco Baiesi, Enrico Carlon, Mario Nicodemi, Bruno Bassetti, Emanuela del Gado, Bianca Sclavi, Kevin D. Dorfman and Andrew Spakowitz for discussions and useful feedback, and to Gino Benza and Ivan Junier for extremely useful comments on this manuscript. This work was supported by the International Human Frontier Science Program Organization, grants RGY0069/2009-C and RGY0070/2014. VFS was funded by a PDI-MSC scholarship of the Institut de recherche pour le développement, Government of France. We acknowledge access to the HPC resources of the Institute for Scientific Computing and Simulation (Equip@Meso project - ANR-10-EQPX- 29-01, Excellence Program "Investissement d'Avenir").

6 Appendix A: Role of loop interactions in the collapse due to sparse bridging.

This Appendix briefly addresses how accounting for loop interactions can improve the estimates for the switch-like collapse presented in Fig. 3A. The scaling of the probability of collapse for swollen arms depends on the excluded volume interaction parameter v through two effects. Firstly, as already mentioned, and accounted in the estimates, the swelling of the arms due to the self-interactions changes the scaling for the contact probability from $P_{\rm loop} \sim g^{-3/2}$ to $P_{\rm loop} \sim g^{-2.27}$[51]. Secondly, and more importantly, there is an interaction, so far neglected between the arms due to the peculiar star-like configuration of the collapsed polymer. The estimates of the switch-like transition from Eqs. 3 and 4 do not show perfect

Soft Matter Accepted Manuscript

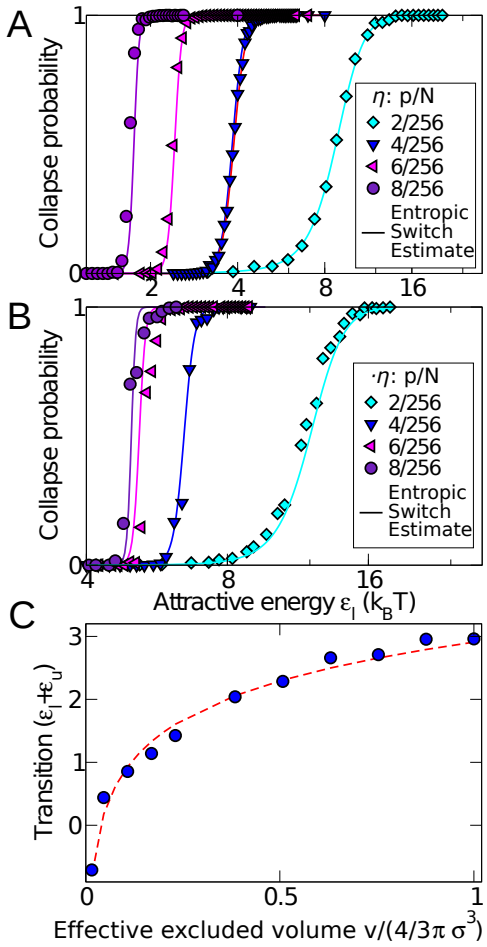

Fig. 8 Role of entropy loss due to loop excluded volume interactions in the collapse due to sparse bridging. A: Collapse of a ghost polymer with bridging interactions. In this case, the inter-arms interactions are absent, and the plot shows good agreement of the predictions of Eqs. 3 and 4 to simulation data. The formulas include a scaling of $P_{\rm loop} \sim g^{-3/2}$ measured from simulations. B: improved theoretical predictions by a shift in the transition energy of value $\Delta S_{star} = a_0(2p-3/2)^{1.68}\log[256/p]$ (see Eq. 11) where $a_0 = 0.00258$ is a fitted parameter. C: Agreement of the scaling of the transition point between the simulations for the polymer with bridging interactions ($p/N = 8/256$) in the swollen arm regime and the predictions of Eq. 5.

agreement with simulations (Fig. 3A) with increasing p because this entropy reduction due to the excluded volume interactions between loops is neglected. This is confirmed by the fact that the approximation of Eq. 4 (valid for sufficiently small p) is very accurate for ghost chains (Fig. 8A).

A loop interaction term must depends on the arm length g as well as from the interaction parameter v and the number of arms f. The entropy reduction for a star polymer with f arms of length N/f has been studied in the thermodynamic limit ($N \to \infty$)[72]. One can define a set of scaling exponents γ_f which define the scaling between the number of configurations of a star polymer made of f arms each of length N/f as

$$Z = \mu^{-N}\,(N/f)^{\gamma_f - 1}\ . \tag{9}$$

Due to the effect of this scaling, the collapse energy of the polymer with bridging interactions is shifted to higher values for increasing p by an entropic contribution as[73]

$$\Delta S_{star} = \sigma_{2p}\log\frac{N}{p-1},\ \text{with}\ \sigma_{2p} = \gamma_p - \frac{\gamma_1+1}{2}\ . \tag{10}$$

Numerical calculations of γ_f for selected values of f have been carried out using field-theoretical methods[72] and lattice polymer simulations[53,74–78].

In a complementary way, the problem of the star polymer has been approached by scaling arguments based on polymer blobs[59]. This approach shows that the scaling of the free energy of the star polymer is proportional to $\sim f^{3/2}$[79], setting a scaling for γ_f. The simulations used to compute γ_f numerically gave[53] the relation

$$\gamma_f - 1 \simeq -(f-3/2)^{1.68} \tag{11}$$

which is in agreement with the scaling estimate.

The simulations and scaling estimates discussed so far do not account for the excluded volume strength. In order to include the role of excluded volume, we propose a scaling for the entropic cost of the star polymer term as in Eq. 5 (see Appendix B), which includes also the logarithmic correction factor depending on the homogeneous interaction term (and containing the parameter v measuring interaction strength). Fig. 8B shows that adding such a term (scaling as Eq. 5) in Eq. 4 sensibly improves the agreement of the theoretical estimate with the simulated switch-like collapse. Fig. 8C specifically tests the role of the logarithmic dependency of the transition point from v, finding satisfactory qualitative agreement.

7 Appendix B: Scaling argument for the entropy of a star polymer.

These notes sketch the calculation of the number of blobs of a star polymer with f arms, each of length N, following Daoud and Cotton[59]. The number of blobs are then used as a proxy for the entropy (blob ansatz). The polymer is described as a series of concentric shells, each of which by definition contains f blobs (one for each arm). The size of the blobs ξ depends on the radial coordinate of the shell (called r). Since the shell at r has surface $\sim r^2$, the size of each blob is $\xi^2 = r^2/f$, which means that $\xi \sim r/f^{1/2}$, i.e. $\xi = ar$, with $a = Cf^{-1/2}$. ξ is also the thickness of the shell at coordinate r.

Starting form a core of size r_0 we now imagine to stack (iteratively) discrete blobs of the proper size on each shell. Each

Soft Matter Accepted Manuscript

This journal is © The Royal Society of Chemistry [year]

stacked shell will determine the coordinate of the following one, and hence its blob size.

$$r_i = a\sum_{k=1}^{i-1} r_k + a\frac{r_i}{2} + ar_0 \ ,$$

with

$$\xi_i = \xi(r_i) = ar_i \ ,$$

leading to the expressions

$$r_n\left(1-\frac{a}{2}\right) = r_0 a(1+a)^{n-1} \ ,$$

and

$$\xi_n = r_0 a^2(1+a)^{n-1} \ .$$

We note now that the relationship $\xi_n \sim g_n^{3/5} v^{1/5} b$, also has to hold (each blob is a swollen polymer of bond length b), where $v = 1/2 - \chi$, and g is the number of monomers in a blob. Hence,

$$g_n = Ae^{\frac{5}{3}(n-\frac{1}{2})a} \ ,$$

where

$$A = \frac{(a^2 r_0)^{5/3}}{v^{1/3} b^{5/3}}.$$

We now follow (on one branch of the star) all the monomers in all the blobs, and impose that their total has to be N. Inverting this relationship gives an estimate for $\beta F \simeq f N_{\mathbf{blob}}$ (since the argument involves the blobs of one arm). One has

$$\sum_{n=1}^{N_{\mathbf{blob}}} g_n = N \ ,$$

hence

$$N \simeq \int_1^{N_{\mathbf{blob}}} \mathrm{d}n A e^{\frac{5}{3}na} \ ,$$

from which

$$N_{\mathbf{blob}} \sim \frac{1}{a}\log Na/A$$

where we neglected additive and multiplicative numerical constants, leading to the expression

$$\beta F \sim f^{3/2} \log\left(N f^{7/6} v^{1/3}\left(\frac{b}{r_0}\right)^{5/3}\right) \ ,$$

which is Eq. (5).

References

1 V. G. Benza, B. Bassetti, K. D. Dorfman, V. F. Scolari, K. Bromek, P. Cicuta and M. C. Lagomarsino, *Rep Prog Phys*, 2012, **75**, 076602.
2 S. C. Dillon and C. J. Dorman, *Nat Rev Microbiol*, 2010, **8**, 185–195.
3 G. Muskhelishvili, P. Sobetzko, M. Geertz and M. Berger, *Molecular BioSystems*, 2010, **6**, 662–676.
4 N. J. Trun and J. F. Marko, *American Society for Microbiology News*, 1998, **64**, 276.
5 J. Stavans and A. Oppenheim, *Physical Biology*, 2006, **3**, R1–.
6 M. S. Luijsterburg, M. C. Noom, G. J. Wuite and R. T. Dame, *J Struct Biol*, 2006, **156**, 262–72.
7 R. L. Ohniwa, Y. Ushijima, S. Saito and K. Morikawa, *PLoS One*, 2011, **6**, e19172.
8 P. A. Wiggins, R. T. Dame, M. C. Noom and G. J. L. Wuite, *Biophys J*, 2009, **97**, 1997–2003.
9 C. A. Brackley, S. Taylor, A. Papantonis, P. R. Cook and D. Marenduzzo, *Proc Natl Acad Sci U S A*, 2013, **110**, E3605–E3611.
10 M. Barbieri, M. Chotalia, J. Fraser, L.-M. Lavitas, J. Dostie, A. Pombo and M. Nicodemi, *Biochem Soc Trans*, 2013, **41**, 508–512.
11 I. Junier, O. Martin and F. Képès, *PLoS Comput Biol*, 2010, **6**, e1000678.
12 W. Wang, G.-W. Li, C. Chen, X. S. Xie and X. Zhuang, *Science*, 2011, **333**, 1445–1449.
13 V. V. Thacker, K. Bromek, B. Meijer, J. Kotar, B. Sclavi, M. C. Lagomarsino, U. F. Keyser and P. Cicuta, *Integr. Biol.*, 2014, **6**, 184–191.
14 D. J. Jin and J. E. Cabrera, *J Struct Biol*, 2006, **156**, 284–91.
15 D. C. Grainger, D. Hurd, M. Harrison, J. Holdstock and S. J. Busby, *Proc Natl Acad Sci U S A*, 2005, **102**, 17693–8.
16 S. B. Zimmerman, *J Struct Biol*, 2006, **156**, 255–61.
17 N. Hadizadeh Yazdi, C. C. Guet, R. C. Johnson and J. F. Marko, *Mol Microbiol*, 2012, **86**, 1318–1333.
18 T. Odijk, *Biophys Chem*, 1998, **73**, 23–9.
19 R. de Vries, *Biochimie*, 2010, **92**, 1715–1721.
20 J. K. Fisher, A. Bourniquel, G. Witz, B. Weiner, M. Prentiss and N. Kleckner, *Cell*, 2013, **153**, 882–895.
21 J. Pelletier, K. Halvorsen, B.-Y. Ha, R. Paparcone, S. J. Sandler, C. L. Woldringh, W. P. Wong and S. Jun, *Proc Natl Acad Sci U S A*, 2012, **109**, E2649–E2656.
22 A. S. Wegner, S. Alexeeva, T. Odijk and C. L. Woldringh, *J Struct Biol*, 2012, **178**, 260–269.
23 A. Javer, Z. Long, E. Nugent, M. Grisi, K. Siriwatwetchakul, K. D. Dorfman, P. Cicuta and M. Cosentino Lagomarsino, *Nat Commun*, 2013, **4**, 3003.
24 S. C. Weber, A. J. Spakowitz and J. A. Theriot, *Phys. Rev. Lett.*, 2010, **104**, 238102.
25 L. A. Mirny, *Chromosome Res*, 2011, **19**, 37–51.
26 X. Wang, X. Liu, C. Possoz and D. J. Sherratt, *Genes Dev*, 2006, **20**, 1727–31.
27 P. A. Wiggins, K. C. Cheveralls, J. S. Martin, R. Lintner and J. Kondev, *Proceedings of the National Academy of Sciences*, 2010, **107**, 4991–4995.
28 M. Valens, S. Penaud, M. Rossignol, F. Cornet and F. Boccard, *EMBO J*, 2004, **23**, 4330–4341.
29 L. Moulin, A. Rahmouni and F. Boccard, *Mol Microbiol*, 2005, **55**, 601–10.
30 O. Espéli and F. Boccard, *J Struct Biol*, 2006, **156**, 304–10.
31 R. T. Dame, O. J. Kalmykowa and D. C. Grainger, *PLoS Genet*, 2011, **7**, e1002123.
32 O. Espéli, R. Mercier and F. Boccard, *Mol Microbiol*, 2008, **68**, 1418–27.
33 C. Lesterlin, R. Mercier, F. Boccard, F. Barre and F. Cornet, *EMBO Rep*, 2005, **6**, 557–62.
34 R. Mercier, M.-A. Petit, S. Schbath, S. Robin, M. E. Karoui, F. Boccard and O. Espéli, *Cell*, 2008, **135**, 475–485.
35 I. Junier, F. Boccard and O. Espli, *Nucleic Acids Research*, 2014, **42**, 1461–1473.
36 L. Postow, C. Hardy, J. Arsuaga and N. Cozzarelli, *Genes Dev*, 2004, **18**, 1766–79.
37 D. Skoko, D. Yoo, H. Bai, B. Schnurr, J. Yan, S. M. McLeod, J. F. Marko and R. C. Johnson, *Journal of Molecular Biology*, 2006, **364**, 777–798.
38 R. Kavenoff and B. C. Bowen, *Chromosoma*, 1976, **59**, 89–101.

Soft Matter Accepted Manuscript

39 A. M. Breier and N. R. Cozzarelli, *Proc Natl Acad Sci U S A*, 2004, **101**, 9175–9176.

40 T. B. K. Le, M. V. Imakaev, L. A. Mirny and M. T. Laub, *Science*, 2013, **342**, 731–734.

41 M. A. Umbarger, E. Toro, M. A. Wright, G. J. Porreca, D. Ba, S.-H. Hong, M. J. Fero, L. J. Zhu, M. A. Marti-Renom, H. H. McAdams, L. Shapiro, J. Dekker and G. M. Church, *Mol Cell*, 2011, **44**, 252–264.

42 C. Cagliero, R. S. Grand, M. B. Jones, D. J. Jin and J. M. O'Sullivan, *Nucleic Acids Res*, 2013, **41**, 6058–6071.

43 M. Barbieri, A. Scialdone, A. Piccolo, A. M. Chiariello, C. di Lanno, A. Prisco, A. Pombo and M. Nicodemi, *Front Genet*, 2013, **4**, 113.

44 M. Fritsche, S. Li, D. W. Heermann and P. A. Wiggins, *Nucleic Acids Res*, 2012, **40**, 972–980.

45 D. W. Heermann, H. Jerabek, L. Liu and Y. Li, *Methods*, 2012, **58**, 307–314.

46 M. Barbieri, M. Chotalia, J. Fraser, L.-M. Lavitas, J. Dostie, A. Pombo and M. Nicodemi, *Proc Natl Acad Sci U S A*, 2012, **109**, 16173–16178.

47 A. Cacciuto and E. Luijten, *Nano Lett.*, 2006, **6**, 901–905.

48 M. G. Noro and D. Frenkel, *The Journal of Chemical Physics*, 2000, **113**, 2941–2944.

49 P. De Gennes, *J. Phyique Lett.*, 1975, **36**, 55–57.

50 M. P. Taylor, W. Paul and K. Binder, *Phys. Rev. E*, 2009, **79**, 050801.

51 D. Marenduzzo, C. Micheletti and P. R. Cook, *Biophys J*, 2006, **90**, 3712–3721.

52 L. Saiz and J. M. G. Vilar, *Curr Opin Struct Biol*, 2006, **16**, 344–350.

53 H.-P. Hsu, W. Nadler and P. Grassberger, *Macromolecules*, 2004, **37**, 4658–4663.

54 L. Leibler, *Macromolecules*, 1980, **13**, 1602–1617.

55 Kantor and Kardar, *Phys Rev Lett*, 1996, **77**, 4275.

56 C. J. Camacho and T. Schanke, *EPL (Europhysics Letters)*, 1997, **37**, 603.

57 N. E. Buchler, U. Gerland and T. Hwa, *Proceedings of the National Academy of Sciences*, 2003, **100**, 5136–5141.

58 A. K. Dasmahapatra, G. Kumaraswamy and H. Nanavati, *Macromolecules*, 2006, **39**, 9621–9629.

59 Daoud, M. and Cotton, J.P., *J. Phys. France*, 1982, **43**, 531–538.

60 O. V. Borisov and A. Halperin, *Macromolecular Symposia*, 1997, **117**, 99–107.

61 O. V. Borisov and A. Halperin, *Macromolecules*, 1996, **29**, 2612–2617.

62 M. Buenemann and P. Lenz, *PLoS One*, 2010, **5**, e13806.

63 T. Curk, F. J. Martinez-Veracoechea, D. Frenkel and J. Dobnikar, *Soft Matter*, 2013, **9**, 5565–5571.

64 T. Curk, F. J. Martinez-Veracoechea, D. Frenkel and J. Dobnikar, *Nano Lett*, 2014, **14**, 2617–2622.

65 Bryngelson and Thirumalai, *Phys Rev Lett*, 1996, **76**, 542–545.

66 F. Benedetti, J. Dorier, Y. Burnier and A. Sasiak, *Nucleic Acids Res*, 2014, **42**, 2848–2855.

67 J. D. Halverson, J. Smrek, K. Kremer and A. Y. Grosberg, *Rep Prog Phys*, 2014, **77**, 022601.

68 S. de Nooijer, J. Wellink, B. Mulder and T. Bisseling, *Nucleic Acids Res*, 2009, **37**, 3558–3568.

69 D. Zickler and N. Kleckner, *Annu Rev Genet*, 1999, **33**, 603–754.

70 C. Lesterlin, E. Gigant, F. Boccard and O. Espeli, *The EMBO journal*, 2012, **31**, 3468–3479.

71 J.-K. Chen and C.-J. Chang, *Materials*, 2014, **7(2)**, 805–875.

72 L. Schäfer, C. von Ferber, U. Lehr and B. Duplantier, *Nuclear Physics B*, 1992, **374**, 473–495.

73 A. Hanke and R. Metzler, *Biophysical journal*, 2003, **85**, 167–173.

74 J. Batoulis and K. Kremer, *Macromolecules*, 1989, **22**, 4277–4285.

75 G. S. Grest, *Macromolecules*, 1994, **27**, 3493–3500.

76 S. Caracciolo, M. S. Causo and A. Pelissetto, *Nuclear Physics B-Proceedings Supplements*, 1998, **63**, 652–654.

77 G. Zifferer, *Macromolecular theory and simulations*, 1999, **8**, 433–462.

78 K. Shida, K. Ohno, M. Kimura and Y. Kawazoe, *Macromolecules*, 2000, **33**, 7655–7662.

79 T. Witten and P. Pincus, *Macromolecules*, 1986, **19**, 2509–2513.

Soft Matter Accepted Manuscript

This journal is © The Royal Society of Chemistry [year]